Automatic Segmentation of the Spine by Means of a Probabilistic Atlas With a Special Focus on Ribs Suppression

Silvia Ruiz-España[1], Juan Domingo[2], Antonio Díaz-Parra[1], Esther Dura[2], Víctor D'Ocón-Alcañiz[1], Estanislao Arana[3], and David Moratal[1*]

[1] Center for Biomaterials and Tissue Engineering, Universitat Politècnica de València, 46022 Valencia, Spain.

[2] Department of Informatics, Universitat de València, 46100 Burjasot, Spain.

[3] Radiology Department, Fundación Instituto Valenciano de Oncología, 46009 Valencia, Spain.

* Corresponding author:

David Moratal

Center for Biomaterials and Tissue Engineering

Universitat Politècnica de València

Camí de Vera, s/n

46022 Valencia, Spain

Tel.: (+34) 96.387.70.07 (ext. 88939)

FAX: (+34) 96.387.72.76

e-mail: dmoratal@eln.upv.es

ABSTRACT

Purpose: The development of automatic and reliable algorithms for the detection and segmentation of the vertebrae are of great importance prior to any diagnostic task. However, an important problem found to accurately segment the vertebrae is the presence of the ribs in the thoracic region. To overcome this problem, a probabilistic atlas of the spine has been developed dealing with the proximity of other structures, with a special focus on ribs suppression.

Methods: The data sets used consist of Computed Tomography images corresponding to 21 patients suffering from spinal metastases. Two methods have been combined to obtain the final result: firstly, an initial segmentation is performed using a fully automatic level-set method; secondly, to refine the initial segmentation, a 3D volume indicating the probability of each voxel of belonging to the spine has been developed. In this way, a probability map is generated and deformed to be adapted to each testing case.

Results: To validate the improvement obtained after applying the atlas, the Dice coefficient (DSC), the Hausdorff distance (HD), and the mean surface-to-surface distance (MSD) were used. The results showed up an average of 10 mm of improvement accuracy in terms of HD, obtaining an overall final average of 15.51 ± 2.74 mm. Also, a global value of 91.01 ± 3.18 % in terms of DSC and a MSD of 0.66 ± 0.25 mm were obtained. The major improvement using the atlas was achieved in the thoracic region, as ribs were almost perfectly suppressed.

Conclusion: The study demonstrated that the atlas is able to detect and appropriately eliminate the ribs while improving the segmentation accuracy.

Key words: Computed Tomography, probabilistic atlas, ribs suppression, vertebral segmentation.

1. INTRODUCTION

The spine is an important anatomic structure that provides protection to the spinal cord, nerves and several organs and gives the body structural support, flexibility and motion. However, this complex structure is subject to a wide variety of diseases that can damage the vertebrae or surrounding tissues changing the structure of the spine and causing, in most of the cases, back pain[1]. Moreover, metastases to the spine represent an important problem in patients with cancer[2]. For nearly half of all advanced cancer patients there is evidence of spinal involvement, associating the vertebral bodies with the highest morbidity and mortality rates[2].

Nowadays, spinal imaging studies are increasing worldwide[3], being Computed Tomography (CT) and Magnetic Resonance imaging (MRI) two of the most common modalities used for the diagnosis of spinal disease. Whereas MRI provides better contrast resolution to differentiate soft tissue structures[4], bony structures are more clearly identified in CT scans allowing an accurate diagnosis of vertebral lesions[5]. Therefore, CT becomes the most preferable imaging modality when there is vertebral involvement in the diagnosis of spinal disorders. Currently, to assist radiologists in the diagnosis task of different abnormalities, computer-aided diagnosis systems are employed, becoming a part of the routine clinical work[6]. Hence, its demand over the past years has increased, becoming an important research topic in medical imaging and also in diagnostic radiology[6,7]. However, due to the high number of pathologies affecting the spine, the segmentation of this structure is essential for many research and clinical studies as it is capable of facilitating disease diagnosis, follow-up assessment, treatment and statistical analysis. Therefore, prior to any diagnosis of spinal disorders or in the study of the disorder, a precise detection and segmentation of the vertebrae are the first crucial steps.

Performing a detailed and robust segmentation is a very challenging task mainly due to partial volume effect, intensity inhomogeneity, intensity similarity and noise. In addition, the segmentation becomes even more complicated because of differences in body structures between individuals, especially in pathological cases. Bone diseases such as metastatic spine cancer alter bone tissue material and geometric properties. They perturb normal bone remodelling process and weaken the structure, resulting in vertebral fractures, deformity, and spinal cord compression, among others. Sometimes, due to increased fragility the tumor may break the cortical shell of the vertebral body. The consequences of these lesions, or other spinal disorders, make difficult to clearly identify the boundaries of the vertebrae and as a consequence to obtain a precise segmentation. Therefore, considerable research effort has been made aiming at developing methods for the automatic or semiautomatic segmentation of the spine from CT scans[8], in both healthy and pathological cases.

The development of methods using prior knowledge of the shape to be segmented is an active field of research[9]. Therefore, most of the developed methods are based on deformable models[10–20], which make use of this information. However, the availability of this kind of data is not always possible, therefore, other methods that do not require any form of prior knowledge are used, too. Some of them are approximations based on thresholding, watershed and direct graph methods[21–23], or level set methods[24–27]. Level-set methods are particularly appropriate for dealing with different features such as cavities or convoluted areas. However, many of these works either do not segment all thoracic and lumbar vertebrae[10–15, 20, 23–26], or they are not completely automatic[10–12, 19, 20, 23, 25], or have been only tested in healthy cases[18, 25]. The presence of the ribs is one of the problems for which different methods show less accuracy in the segmentation of the thoracic region[16, 21, 27–29]. This is mainly due to the difficulty of discriminating between these structures and the vertebrae. However, most of the problems leading to back pain are related to lumbar region, as this area supports the greatest load of the spine. This is the reason why the majority of studies have only been focused on this region[10–12, 15, 20, 23–25]. Despite that, several studies found in the literature have made a great effort to segment all thoracic and lumbar vertebrae[16–19, 21, 22, 27–29], but in most of the cases, the results obtained were more successful in segmenting the lumbar region. A possible solution to overcome this problem is to use an atlas-based segmentation.

The atlas is a way to introduce anatomical information related to the position of an organ. Two main different types of atlases have been proposed in the medical imaging literature. On one hand those based on shape variations, whose result is a set of binary 3D shapes representing the prototypical shape (mean) and different modes of variation. On the other hand, those in which each voxel has a real value representing either the confidence or the probability of such a voxel of being part of the structure of interest. The first type, normally known as statistical atlas, is usually constructed by using techniques of Principal Component Analysis (PCA) using as input data the spatial coordinates of a set of relevant points (landmarks) chosen either manually or automatically[30, 31]. The second type, probabilistic atlases, utilizes techniques based on mathematical morphology and probabilistic models[32–34].

With both approaches, considerable research effort has been directed towards the construction of brain atlases[35]. A variety of methods have been also proposed for the segmentation of other organs or anatomical structures by means of atlases[36–42]. However, the number of studies related to the construction of spinal atlases is limited and some of them are centred on structures like the intervertebral discs[43] or the spinal canal[44, 45]. Regarding vertebrae, Hardisty et al.[46] presented an algorithm to perform the segmentation of tumor-involved vertebrae using demons deformable image registration and level set methods. However, the algorithm is not fully automatic, being necessary user interaction to align the atlas with the scan of interest. In addition, authors did not take into account all thoracic vertebrae. Forsberg[47] performed an atlas-based registration for the segmentation of all thoracic and lumbar vertebrae but they did not include any pathological spine in the data sets.

In this paper we are particularly interested in probabilistic atlases. However, by using only atlas-based segmentation methods it is difficult to capture the fine details or localize areas with high cavities in complex images, mainly due to the anatomical variability. Therefore, in this study two different methods have been combined; firstly, an initial segmentation of each vertebra is performed using a level-set based segmentation method[27]. Secondly, a probabilistic atlas of the spine has been developed, including the last cervical vertebra and the entire thoracic and lumbar regions, generating a probability map that it is deformed to be adapted to each patient. To the best of our knowledge, this is the first time that an atlas has been implemented in order to refine an initial segmentation dealing with the proximity of other structures, with a special focus on ribs suppression. In addition, the entire process is fully automatic and it has been tested in pathological spines. A general approach of the whole method is shown in Fig. 1.

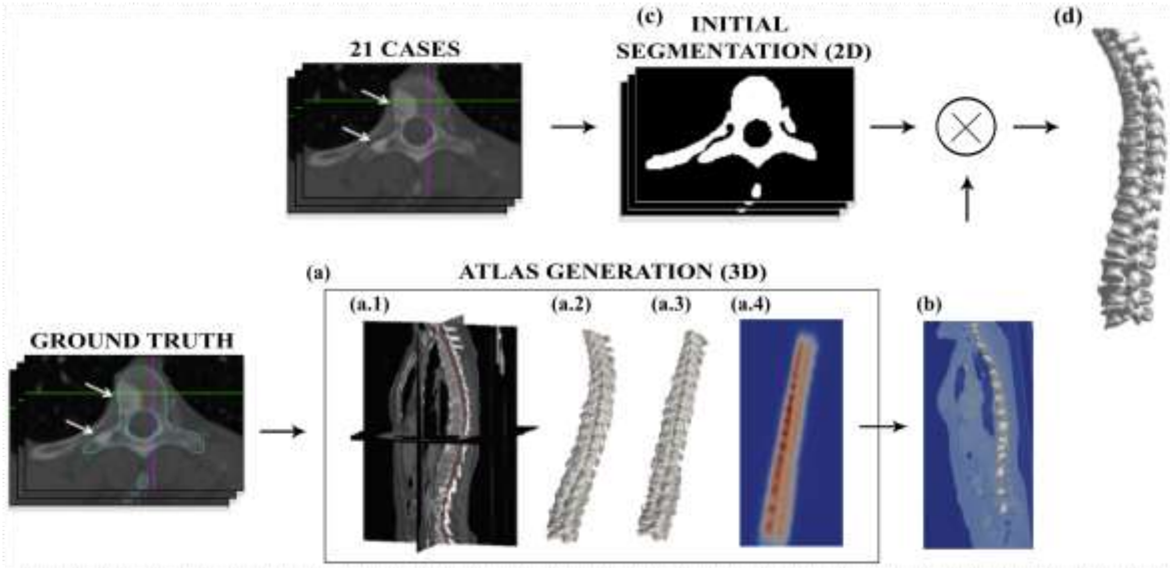

FIG. 1. General approach of the presented method. Twenty-one cases have been selected and manually segmented by an experienced radiologist (ground truth). 21 atlases have been built using 20 cases each and used to segment the remaining case (leave-one-out test). A vertebra with focal osteoblastic lesions in the left side is shown (see white arrows). (a) Atlas construction by means of the ground truth data (performed in 3D). (a.1) Curves representing the global length and shape of the spine. (a.2) Binary shapes of the segmented spines used to construct the atlas. (a.3) Geometric transformation applied (straight spines) to perform the registration of the binary shapes of the segmented spines. (a.4) Probability map generated (atlas) that indicates the probability of each voxel to belong to the spine. Blue color represents a lower probability and red color a higher probability. (b) Deformation of the atlas to be adapted to each testing case. The atlas has been thresholded and the outer surface is shown. (c) Initial segmentation performed to each testing case using level set method (performed in 2D). (d) Refinement of the initial segmentation using the atlas to obtain the final result.

2. MATERIALS AND METHODS

2.A Subjects and Data Sets

In this study, 21 patients suffering from spinal metastases were selected. In total, the sample included 11 male and 10 female (58.47 ± 13.78 years, mean ± standard deviation) and the data sets used consisted of CT images acquired on a Siemens Sensation 40 (Siemens, Erlangen, Germany) scanner at Fundación Instituto Valenciano de Oncología.

These scans covered the last cervical and all thoracic and lumbar vertebrae. Images were reconstructed with a standard filtered back projection algorithm, using a soft kernel (B20). The in-plane resolution for these images ranged from 0.7031 to 0.9648 mm with a slice thickness of 2 or 2.5 mm. The matrix size was 512 × 512, with a total number of slices varying from 291 to 477.

An expert manually segmented the vertebrae of all cases. A total of 6103 slices were segmented. In addition, several programs were written for atlas construction and geometric deformation using C++ and the ITK libraries[48] with calls to routines in the R language, particularly the locfit library[49].

2.B Spinal Atlas Construction

2.B.1 Probabilistic Atlas

Regarding atlases, there are two important aspects to point out. First, the initial raw data are examples of correctly segmented binary shapes. The procedure of segmentation is of crucial importance to obtain a good atlas, so manual or assisted segmentation should be used. This is the reason why manually segmented data performed by an expert has been used in this work.

Another extremely important point is co-registration of the binary shapes of the sample.

Several models for registration can be chosen, from the simplest ones (rigid transformations composed by a translation plus a rotation) to the most complex and flexible models like local deformations. A point of balance between excessively rigid and widely flexible registration can be found through the use of anatomical landmarks that guide the registration. This will be explained in detail in section 2.B.3.

In this study, we focus on the use of a probabilistic atlas, a 3D volume indicating the probability of each voxel of belonging to a prototype shape, the spine in this case. Some segmentation algorithms can interpret this as an a-priori probability and use Bayesian methods to update it using the values of the signal at that voxel or at neighbour ones as new information[34]. Other algorithms can interpret it as a possibility of belonging to a set of voxels that constitute the relevant structure and rely on fuzzy techniques[43] and, finally, others can use the values as initial function to apply level-set techniques[46]. Section 2.B.2 explains how our probabilistic atlas has been built together with the applied improvement to get a more accurate result.

The prevalent idea used up to now for the construction of a probabilistic atlas is simply to register the binary shapes in the sample and look at each voxel to see how many of the shapes cover it. This, divided by the number of shapes in the sample, is a crude measure of the probability of that voxel of belonging to the ideal shape. This is used for example in the works of Park et al.[34, 50]. In this work, this has been formalized as the coverage function.

Other possibilities for building probabilistic atlases use the distance function and transformations of it. Intuitively, the distance function associated to a binary shape is a function from the 3D space to the real numbers and measures how far each point is from the shape. There are two variants: unsigned distance function, for which points inside the shape are considered at distance zero and those outside get the distance to the closest point of the shape surface; and signed distance function, for which every point gets the distance to the closest point on the surface of the shape, with negative sign for those points inside the shape. There are few approaches that use the distance function to build atlases; a relevant one is the work of Pohl et al.[51] that, using a logistic link function, transforms a signed distance map into a log-odds map.

The main idea presented in this paper regarding atlas construction, is the combination of both approaches, the coverage function and the distance function, using a generalized linear model (GLM).

2.B.2 Construction of the Probabilistic Atlas

As stated previously, the most widely used approach of building a probabilistic atlas consists on aligning all the shapes and seeing how many shapes cover each voxel. The formalization uses concepts of random sets. Intuitively, a random set is a statistical distribution whose realizations are n-dimensional sets of points. Let *F* be a random compact set whose realizations are binary shapes: compact (but not necessarily convex) sets of points of R^3 (in general of R^d). Our random set will be a generic spine whose realizations are the shapes of the spine of each patient. Given any fixed shape S, which is for us each of the manually segmented shapes (spines), and for any point $x \in R^d$, $1_S(x)$ will denote the set indicator function, i.e.:

$$1_s(x) = \begin{cases} 1 & if \quad x \quad \in S \\ 0 & if \quad x \quad \notin S \end{cases} \qquad (1)$$

In any random compact set *F*, value $1_s(x)$ is a random variable that takes values in the binary set $\{0,1\}$. Now, let us consider a random sample of *F*, i.e. a collection of independent and identically distributed (as *F*) random compact sets $\Phi_1,\ldots,\Phi_n$, being

$\phi_1, \dots, \phi_n$ the corresponding realizations. Having these data an unbiased estimator for the coverage function $c(x)$ is:

$$\hat{c}(x) = \sum_{i=1}^{n} 1_{\phi_i}(x) \tag{2}$$

which has a clear intuitive meaning: the number of shapes in the sample to which point x belongs (in real terms: an estimation of for how many cases this point belongs to the spine). The coverage function offers a way to calculate an unbiased estimator for the probability $p(x)$:

$$\hat{p}_1(x) = \sum_{i=1}^{n} \frac{1_{\phi_i}(x)}{n} \tag{3}$$

$p(x)$ corresponds to the classical probability as number of hits over total number of cases. Its threshold below 0.5 is related with the concept of mean shape, and indeed it is a particular case of the so-called Vorob'ev mean[52]. But this definition for $p(x)$ has some drawbacks mainly related to the fact of estimating the probability at each point in isolation, as if the random variable that is the coverage at that point was independent of all other points. This makes the thresholds below a given value of $p(x)$ (which are binary shapes) rougher than it would be expected of a summary shape. A feasible alternative to solve this problem consists in using the distance function; concretely, on finding a sensible relationship between the probability and the value of the distance function at a given point or at some related points. The formal definitions are as follow: given a binary shape, *S*, $d_s(x)$ will be the distance function to *S*:

$$d_s(x) = \begin{cases} min_{y \in \partial S} d(x,y) & if \;\; x \notin S \\ 0 & if \;\; x \in \partial S \\ -min_{y \in \partial S} d(x,y) & if \; x \; \in int(S) \end{cases} \tag{4}$$

where $d(x,y)$ is the Euclidean distance between x and y, ∂S the boundary of S and $int(S)$ the interior of the set *S*. This function is calculated at every point of the digital grid for each voxel in every segmented spine. In a similar way, d_{Φ} can be defined not for a fixed set but for a random set F. In this case, $d_{\Phi}(x)$ is a random variable. Since $1_{\Phi}(x) = 0 \Leftrightarrow d_{\Phi}(x) > 0$ and $1_{\Phi}(x) = 1 \Leftrightarrow d(x) \leq 0$, $d(x)$ univocally determines $1_{\Phi}(x)$. Let

$$p(x) = E\left(1_{\Phi}(x)\right) = P(x \in \Phi) \tag{5}$$

where E is the expectation over all sets in F. From here the mean distance function $d^*_{\Phi}(x)$ is defined as

$$d^*_{\Phi}(x) = Ed(x, \Phi). \tag{6}$$

In practice, the mean distance function is estimated for a collection of samples $\phi_1, \dots, \phi_n$ as

$$\hat{d}^*_{\Phi}(x) = \sum_{i=1}^{n} \frac{d_{\phi_i}(x)}{n}. \tag{7}$$

The intuitive meaning of this function of the special location x is the average distance from point x to the border of the mean shape for any shape of the sample. Similarly to the mean coverage, the threshold below some value of the mean distance function gives a binary shape that can also be considered as a mean shape, being this time 0 the natural threshold (a definition derived from the so-called Baddeley-Molchanov mean[53]). The mean distance function is smooth and therefore its thresholded versions are smoother than those of the mean coverage function. This is why the function $p(x)$ will be estimated using information about the mean distance function.

Our hypothesis assumes that $p(x) = f\left(d^*(x)\right)$ (i.e.: the probability is directly linked to the mean distance function) and the link between them must be found. Since $d^*(x)$ can be positive or negative the natural link in the context of General Linear Models consists in using a cumulative distribution function (c.d.f.), which is a non-decreasing function $F: R \longrightarrow [0,1]$. The value $d^*(x)$ is commonly transformed using a basis of functions denoted as $v(x) = \left(1, v_1\left(d^*(x)\right), \dots, v_{p-1}\left(d^*(x)\right)\right)'$, being t' the transpose of the vector t. The model to be assumed is:

$$p(x) = F\left(\beta' v(x)\right) \tag{8}$$

being $\beta' = \left(\beta_0, \beta_1, \dots, \beta_{p-1}\right)$ a vector of coefficients to be determined. In GLM the common choices for the link function F are the c.d.f. of either the standard logistic distribution or of the standard normal distribution. The first one will be used, i.e.:

$$p(x) = \frac{e^{\beta' v(x)}}{1 + e^{\beta' v(x)}}. \tag{9}$$

For any given point x_0, it is expected $p(x)$ be a smooth function so it can be assumed that $p(x)$ takes a constant value in a ball centred at x, $B(x_0, h)$ with radius $h > 0$. Let $\left(x_j, 1_{\phi i}(x_j)\right)$ with $j = 1, \dots, J$ be the points within $B(x_0, h)$. In this way the local pseudo-likelihood function for the *i-th* realization ϕ_i is given by

$$\prod_{j=1}^{J} w\left(x_j, x_0\right) p\left(x_j\right)^{1_{\phi i}(x_j)} \left(1 - p\left(x_j\right)\right)^{1 - 1_{\phi i}(x_j)} \tag{10}$$

using a w-function $w(x, x_0) = K(\|x - x_0\|/h)$ with K a kernel function modulated by a bandwidth h. Accordingly, the whole likelihood function for a complete random sample of F will be:

$$l(\beta) = \prod_{i=1}^{n} \prod_{j=1}^{J} w\left(x_j, x_0\right) p\left(x_j\right)^{1_{\Phi i}(x_j)} \left(1 - p\left(x_j\right)\right)^{1 - 1_{\Phi i}(x_j)} \tag{11}$$

and its log-likelihood will be:

$$l(\beta) = logL(\beta) = \sum_{i=1}^{n} \sum_{j=1}^{J} \left(log\left(w\left(x_j, x_0\right)\right) + 1_{\Phi i}\left(x_j\right) log\left(p(x_i)\right) + \left(1 - 1_{\Phi i}\left(x_j\right)\right) log\left(1 - p\left(x_j\right)\right)\right) \tag{12}$$

This global likelihood will be maximized by a vector of parameters, that will be denoted by $\hat{\beta}(x_0)$, i.e.:

$$\hat{\beta}(x_0) = argmax_{\beta} l(\beta). \tag{13}$$

Determination of $\hat{\beta}$ is done by the optimization methods provided by the R locfit package[49]. The final estimator proposed for the probability function $p(x)$ is:

$$\hat{p}(x_0) = \frac{e^{\hat{\beta}(x_0)' v(x)}}{1+e^{\hat{\beta}(x_0)' v(x)}} \tag{14}$$

Its value at location x_0 is our probabilistic atlas. The estimation procedure can also provide as an output simultaneous confidence bands, i.e. an estimation of the 95% confidence interval around the value at x_0. This possibility will not be used in this work.

2.B.3 Anatomically-Guided Registration for Spine

The process of co-registration is a key point with substantial influence on the final results. A too rigid registration (a method with few free parameters which allows only limited changes, like rigid transformations) preserves well the variability (shape changes present in the sample) but gives a poor shape representation, not similar to the typical shape expected for the organ or structure. On the other hand, a too flexible registration (a method with many free parameters which allows global and local deformations) makes the shapes fit almost perfectly to one of them or to a predefined model, but annihilates the variability. In this way, the probabilistic atlas is not a probability any more but a set with only two possible values, 0 and 1, like a binary shape.

An appropriate balance between flexibility and variability is a complex issue that cannot be deeply treated here. However, a suitable solution is to use a relatively flexible method guided by anatomical knowledge, i.e.: driven by a set of known anatomical landmarks that limit the free deformation, otherwise introduced by local deformation methods. Unfortunately, this is not always possible due to the difficulty of performing a reliable detection and consistent matching of a sufficient number of landmarks. But in the case of the spine, the spinal canal can be reliably detected. The location of its centers at all the different heights make a 3D curve that represents the global length and shape of the spine. For this purpose, an algorithm that combines 2D and 3D information was used[54]. Briefly, this algorithm is composed of three main stages and it is based on the fact that the spinal canal is surrounded by cortical bone. Firstly, a thresholding and a set of morphological operations were applied to set a high contrast between spinal canal and cortical bone. Secondly, only 3D connected objects forming part of the spinal canal were extracted. Finally, a centroid extraction for each slice of the spinal canal object was computed. Further details on this algorithm can be found in Ref. 54. Therefore, using this method the centre points of the spinal canal at each slice were extracted, obtaining a set of 3D points that were used to create the 3D curve previously mentioned.

The main idea proposed in this work is that a good co-registration of two different spines can be attained by deforming one of them so that these curves coincide. Nevertheless, in the case of the atlas construction we want to co-register not only two spines but all the cases in the sample. At this point arises the typical problem of to which of the available cases should the others be registered. Instead of choosing one of them, the registration will be done so that all the 3D curves, obtained from the 3D points previously detected in the spinal canal, coincide with a straight segment of unitary length, creating effectively an abstract model space in which the atlas will be constructed[16, 55]. The concrete procedure to get these geometrical transformations relies on curve fitting, the Frenet trihedron and a chain of rigid transformations that will be explained next.

Let us call $V = \{v_0, v_1, \dots, v_T\}$ *a* succession of points of R^3 with $v_i = (x_i, y_i, z_i)$ obtained as the centres of the vertebral canal at each slice of the CT data set. Considering the z-axis in the direction of the image axis (slices perpendicular to it) and pointing upwards, it is always true that $z_i > z_{i-1}$. The first step is to get a fit of these points to a set of B-splines (polynomials that generate the smooth 3D curve that best fits to all the points and which has also smooth derivatives). The curve is a function:

$$f: [a..b] \longrightarrow R^3 i.e.: f(t) = \big(x(t), y(t), z(t)\big) \quad (15)$$

It depends on an scalar parameter, *t*, which will be normalized in [0..1] so that $f(0) = v_0 = (x_0, y_0, z_0)$ and $f(1) = v_T = (x_T, y_T, z_T)$. The value of the curve parameter corresponding to point v_i will be called t_i so that $f(t_i) = v_i$. Fitting the curve to a set of B-splines allows an analytic representation of it, whose derivatives can be explicitly calculated and evaluated at any point. Specifically, *f* will be used to calculate the tangent vector at each point of the curve, which is simply:

$$\vec{T}(t) = \left(\frac{dx(t)}{dt}, \frac{dy(t)}{dt}, \frac{dz(t)}{dt}\right) \quad (16)$$

It is also possible to calculate the normal and binormal vectors. However, because of noise they were not used in the registration process. Instead, it will be assumed that the spinal canal lays on a vertical plane so that the normal vector is approximately the same for all the points, and will be taken as the vector normal to the plane at minimal perpendicular distance of all points. This vector will be called $\vec{n}$. The tangent vector, on the contrary, is different at each point.

The geometrical global transformation proposed is a succession of rigid transformations (translation plus rotation), each of them applied to a different slice. Let *SL* be the set of slices, $SL = \{sl_0, \dots, sl_T\}$ where sl_i is the intersection of the whole volume with a plane that contains the point v_i and whose normal vector is $\vec{T}_i$. The local coordinate system of this slice has its z-axis coincident with $\vec{T}_i$ and its y-axis coincident with vector $\vec{n}$. See Fig. 2.

Finally, slice sl_i will be transformed so that its origin goes to point $(0,0,t_i)$, its z-axis

$\overrightarrow{T}(t_i)$ becomes $\vec{Z} = (0,0,1)$ and its y-axis $\vec{n}$ becomes $\vec{Y} = (0,1,0)$. This means that the slanted plane sl_i becomes a horizontal plane and the whole spine resembles a straight spine after the transformation. Notice that with this approach the size gets normalized, since the length along the curve (parameter t) is normalized in $[0\ldots1]$ and the small variations in orientation (tilt) are unified because of the use of a common normal vector, $\vec{n}$.

The registration obtained with this specific approach is, at least visually, very good but results will have to be demonstrated by the usefulness of the atlas built when applied to the segmentation task.

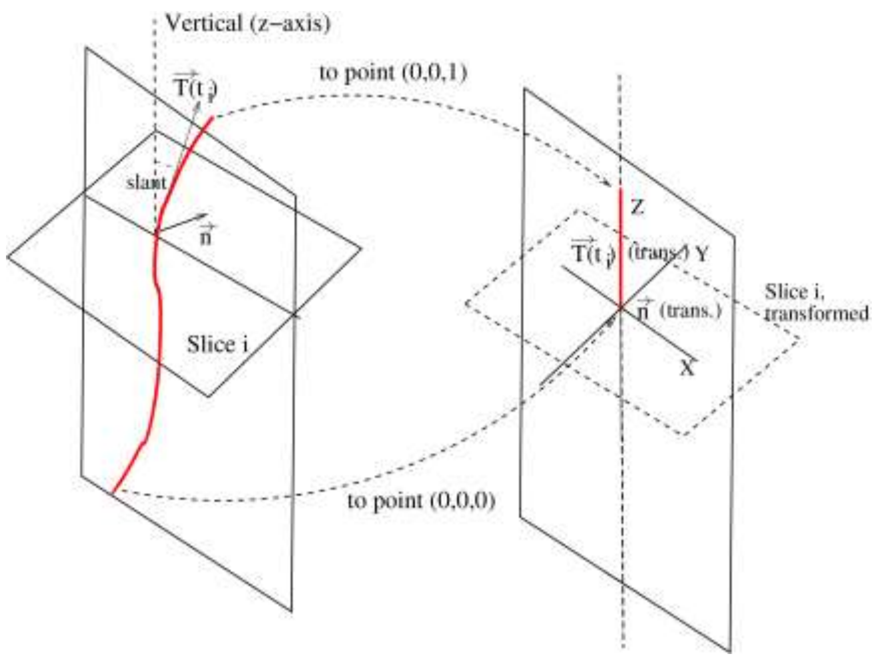

FIG. 2. Schema of the geometric transformation applied to each slanted slice.

2.C Segmentation

2.C.1 Initial Segmentation

To perform the initial segmentation of the vertebrae, a level-set based segmentation method[27] was used. Concisely, four main steps were carried out per slice (see Fig. 3).

Firstly, the detection of a seed point is a necessary step to automate the whole process. For this purpose, the same algorithm used for the spinal canal detection in the atlas construction was applied[54]. In this way, the centre points of the spinal canal extracted at each slice were used as seed points to generate the initial contours. Secondly, to improve image quality a processing step was performed. This step included the generation of a region of interest from the seed points previously detected, the application of a soft tissue window to obtain a high contrast between bone and soft tissues, and the application of a gamma correction to improve brightness and contrast of the images. Third step was to perform the segmentation using the Selective Binary Gaussian Filtering Regularized Level Set method[56]. In the last step two morphological operations were applied: extraction of the 3D object with the highest number of voxels and a hole filling technique.

This method was used to segment all the vertebrae corresponding to all patients used in this study (Fig. 1(c)).

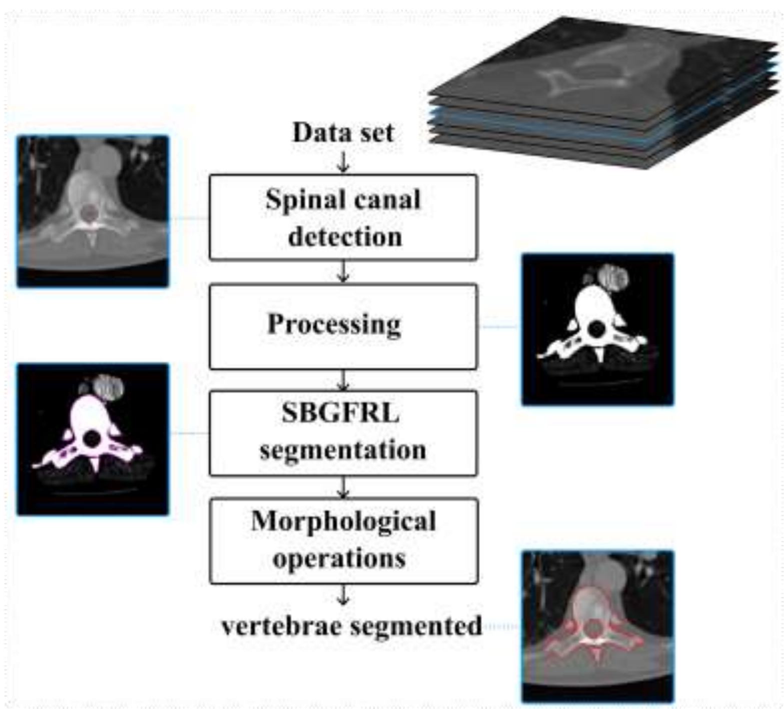

FIG. 3. Flowchart of the level-set -based segmentation method.

2.C.2 Atlas-Based Segmentation

Once the initial segmentation was performed, next step was to refine the segmentation process in order to eliminate the ribs or even other structures that initial segmentation was not able to appropriately eliminate. To achieve this goal, an atlas-based segmentation of each case, using the atlas that has been constructed using the remaining patients (Fig. 1(b)), was performed and combined with the initial segmentation obtaining the final result (Fig. 1(d)).

First of all, the use of the atlas in segmentation requires its registration with the testing case; this involves the detection of the vertebral canal in the new case and the adaptation of the unitary length segment of the atlas to it. To this end, the geometric transformations used for the initial co-registration were conversely applied to the atlas.

Next, to perform the atlas-based segmentation a threshold was applied to it so that points with probability below the threshold were ruled out. Threshold determination is a delicate point, which needs special methods. 21 different atlases were built using for each atlas 20 cases and leaving out one case (leave-one-out method). Each manually segmented slice of the case not used to build each atlas was compared in terms of Hausdorff distance with the corresponding atlas slice, thresholded at every possible level; the optimal values were selected, obtaining in this way the optimal threshold for each case and slice. The average per slice of the thresholds obtained for all cases was plotted as a function of the normalized slice height and adjusted to an analytical function. Given the shape of the raw data, a sigmoidal function seemed a suitable choice. This is shown in Fig. 4, which shows the raw data and the adjusted function for each slice depending on its normalized height (height values in 0..1 along the spinal canal).

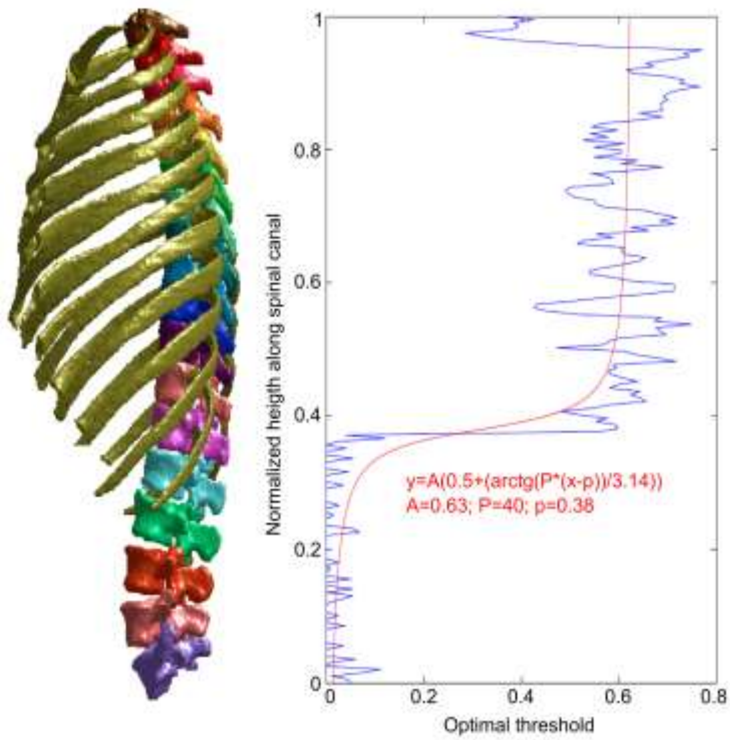

FIG. 4. Optimal threshold to be applied to each slice of the atlas as a function of the normalized height along the spinal canal. Blue line corresponds to the raw data and red line to the adjusted function.

2.C.3 Evaluation of Segmentation

To evaluate the segmentation results and the improvement obtained after applying the atlas to the initial segmentation, the Dice similarity coefficient (DSC)[57], the Hausdorff distance (HD)[58] and the mean surface-to-surface distance (MSD)[59] were used.

The DSC is defined as:

$$\mathrm{DSC}(\Omega_{GT}, \Omega_S) = \frac{2*|\Omega_{GT} \cap \Omega_S|}{|\Omega_{GT}| + |\Omega_S|} \quad (17)$$

where $|\Omega_S|$ and $|\Omega_{GT}|$ represent the volumes in voxels of the segmented object (Ω_S) and the ground truth (Ω_{GT}). The value of DSC denotes the similarity between two volumes and ranges from 0 to 1, being 0 the worst match and 1 the best match.

On the other hand, the HD is defined as:

$$\mathrm{HD}(A,B) = max\big(h(A,B), h(B,A)\big) \quad (18)$$

where

$$h(A,B) = max_{a\epsilon A} min_{b\epsilon B} \|a-b\| \quad (19)$$

A and B are the boundaries of the segmented object and of the ground truth respectively, and $h(A,B)$ is called the direct HD from set A to set B. The value of HD indicates the difference between two surfaces. If the value is 0 means that both volumes share the same boundary, a larger value of HD means a larger distance between boundaries.

Finally, the MSD is defined from its symmetrized version. The formulae are

$$SSD(S,S') = \sqrt{\frac{1}{|S|}\sum_{i=1}^{|S|} d(p_i,S')^2} \quad (20)$$

$$MSD(S_r,S_s) = max[SSD(S_r,S_s), SSD(S_s,S_r)] \quad (21)$$

being S and S' two surfaces, $|S|$ the number of points in a surface S and $d(p_i,S')$ the minimum distance between point $p_i \in S$ and surface S'. See the work described by Aspert et al.[59].

In summary, a good segmentation will be obtained for high values of DSC and low values of HD and MSD.

3. RESULTS

3.A Segmentation Results

The effectiveness of the method was evaluated by applying it to every case with a leave-one-out test. An atlas was built using 20 cases which is then employed to segment the remaining one.

Numerical results are provided in Tables I, II and III, whose columns compare the segmentations obtained with and without the atlas, both for the whole spine (thoracic and lumbar regions) and for each region separately, with the manual segmentation (ground truth). This comparison is shown in terms of DSC in Table I, in terms of HD in table II and in terms of MSD in table III.

TABLE I. Comparison between automatic segmentation (without and with atlas) and ground truth in terms of DSC.

	Dice coefficient [%]					
	Global		Thoracic spine		Lumbar spine	
	without atlas	with atlas	without atlas	with atlas	without atlas	with atlas
Minimum value	86.79	82.61	83.94	75.60	90.99	90.80
Maximum value	92.76	94.21	90.20	92.48	97.17	97.17
Mean value	90.48	91.01	87.53	88.22	95.26	95.23
Standard deviation	1.61	3.18	1.51	4.41	1.88	1.94

TABLE II. Comparison between automatic segmentation (without and with atlas) and ground truth in terms of HD.

	Hausdorff distance [mm]					
	Global		Thoracic spine		Lumbar spine	
	without atlas	with atlas	without atlas	with atlas	without atlas	with atlas
Minimum value	21.51	11.76	21.51	11.09	4.27	4.27
Maximum value	32.30	23.41	32.30	23.41	20.78	17.59
Mean value	25.39	15.51	25.39	14.93	10.42	10.24
Standard deviation	3.19	2.74	3.19	3.05	4.61	4.18

TABLE III. MSD from the automatic segmentation (without and with atlas) to the ground truth

	Mean surface-to-surface distance [mm]					
	Global		Thoracic spine		Lumbar spine	
	without atlas	with atlas	without atlas	with atlas	without atlas	with atlas
Minimum value	0.74	0.41	1.00	0.57	0.15	0.15
Maximum value	1.16	1.38	1.45	1.96	0.67	0.67
Mean value	0.90	0.66	1.24	0.87	0.33	0.33
Standard deviation	0.12	0.25	0.14	0.35	0.14	0.15

As Table I shows, the variation in terms of DSC at the global level, after applying the atlas, is quite modest (about 0.53 % better). In this case, the differences between the segmentation obtained without the atlas and using the atlas are not statistically significant (*t*-test, p=0.2875). Nevertheless, the difference in HD (Table II) highlights the main improvement: the elimination of the ribs in the thoracic region, which cannot be suppressed unless anatomical knowledge about their location is used. These ribs account for less than 2 % of the total spine volume (hence, the minimal DCS variation) but HD decreases about 10 mm on average (from about 25 mm to 15 mm). Results show a statistically significant improvement in segmentation (*t*-test, p<10-8). In addition, Table III shows the precision of the method by obtaining a final MSD of 0.66 ± 0.25 mm for the whole spine. In this instance, the differences between segmentations are also statistically significant (*t*-test, p=7.3641e-05). Besides, all the improvement of using the atlas is concentrated at the thoracic region, since results were already very good (DSC=95 %, HD=10 mm and MSD=0.33 mm) in the lumbar region.

The graphical result in Fig. 5, that corresponds to a typical case, clearly confirms this improvement in the thoracic region. This figure shows, from left to right, the manual segmentation, the segmentation using the level-set method (initial segmentation), the final segmentation (refinement with atlas), the difference between initial and final segmentations and the difference between manual and final segmentations, after morphological opening with a ball of radius 1 to highlight the differences.

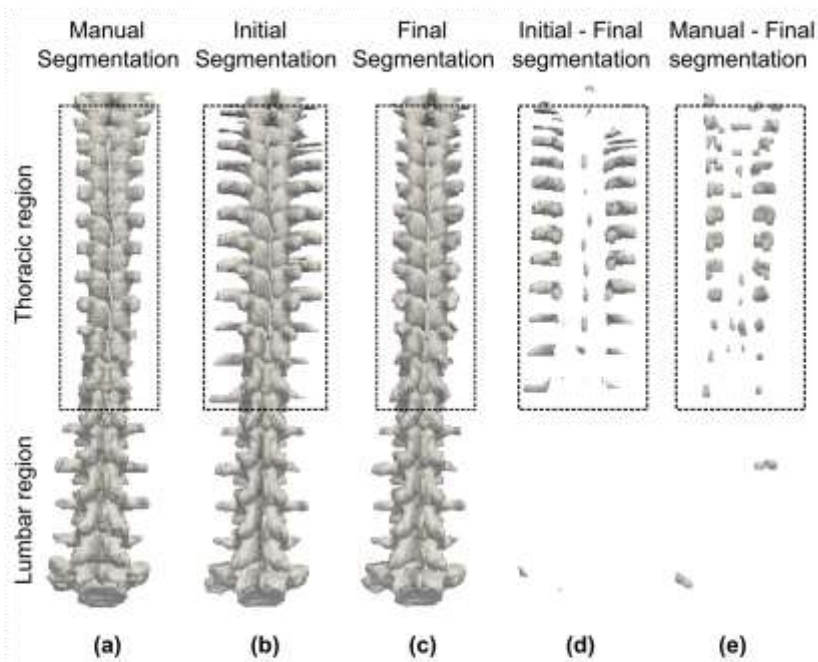

FIG. 5. (a) Manual segmentation (ground truth data). (b) Initial segmentation (without the atlas). (c) Refinement of the initial segmentation using the atlas. (d) Difference between (b) and (c). (e) Difference between (a) and (c). Thoracic regions are outlined by the dotted black lines.

To observe in more detail the segmentation result and its improvement, 2D images corresponding to the segmentation process in one slice for each of the two regions are shown in Fig. 6.

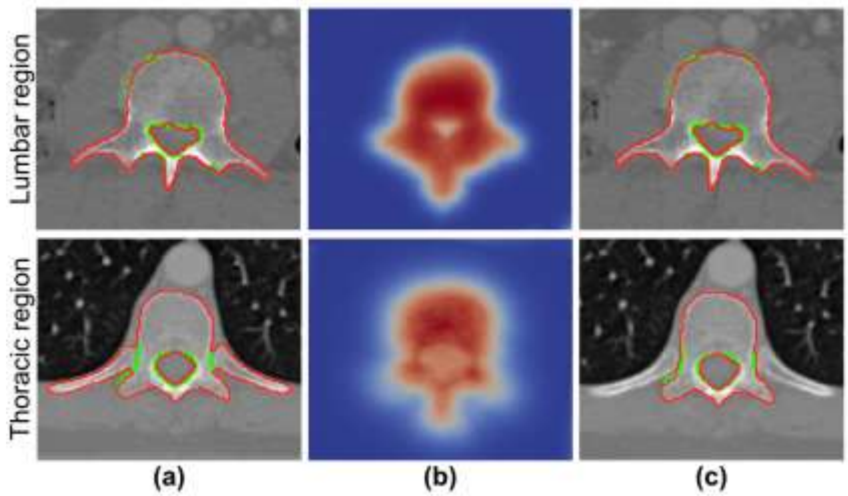

FIG. 6. Segmentation process of two slices. (a) Initial segmentation (without atlas). (b) Probability map. Colors indicate probability of each voxel to belong to the spine (blue as lower and red as higher probability). (c) Final segmentation (with atlas). Red lines correspond to the automatic segmentation and green lines to the ground truth.

3.B Computational Workload

The computational cost of the method is mainly related with the step of atlas construction. The need to calculate the distance functions and the application of the linear model consume most of the time. Using a computer with an Intel Xeon at 2.67 GHz and with 24 GB of RAM, distance function took about 2 minutes per case and atlas construction about 7 minutes. The calculations of the distance functions could be done separately and therefore in parallel for each case, reducing in this way the time needed. Nevertheless, atlas is built only once and used later to segment every new case, so the time spent in atlas construction is not as relevant as the time needed for segmentation. In the proposed method, the whole process of segmentation including spinal canal detection (50 seconds), initial segmentation

(1 minute), atlas deformation and refinement of the first-step segmentation (2 minutes) took only 4 minutes per case.

4. DISCUSSION

Considerable research effort has been directed towards the segmentation of a specific region of the spine, specially the lumbar region. Our method achieved in this region an average of 95.23 ± 1.94 % in terms of DSC and an average of 10.24 ± 4.18 mm in terms of HD, better values than those obtained in previous works[15, 25, 26]. The method proposed by Huang et al.[24] achieved a little better HD but the DSC was less accurate. An accuracy of 0.98 was obtained combining deformable models with the geometrical shape of the vertebral body[11]. However, in this work the authors only segmented three lumbar vertebrae and the algorithm required user interaction. The method used by Rasoulian et al.[12] obtained a better HD (8.91 ± 2.42 mm) than ours, but the MSD (1.38 ± 0.56 mm) was considerably higher compared to the proposed method applied in the lumbar region (0.33 ± 0.15 mm). The method introduced by Pereañez et al.[20] achieved also a higher MSD, with a value of 1.15 ± 0.10 mm.

However, many errors in vertebral segmentation are obtained in the thoracic region because of the presence of the ribs. Considering both regions, the described method obtained an average of 91.01 ± 3.18 % in terms of DSC and an average of 15.51 ± 2.74 mm in terms of HD, values a slightly better than those obtained previously[27]. The method proposed by Castro-Mateos et al.[19] achieved a marginally smaller HD for pathological subjects, but the DSC was not as accurate. Stern et al.[17] and Korez et al.[18] achieved slightly better values for their algorithms. However, Korez et al.[18] did not tested the algorithm in patients with spinal deformities. On the other hand, Stern et al.[17] segmented each vertebra separately, the same as other authors[11, 13–15], which might lead to missegmentation because of the ambiguous boundaries between vertebrae. Klinder et al.[16] tried to avoid this problem proposing a simultaneous segmentation of all vertebrae. However, their algorithm for the identification of the vertebral bodies was very computationally expensive (20-30 minutes per case). Regarding the MSD, in Table III can be appreciated that this measure was clearly improved after applying the atlas. A mean value of 0.66 ± 0.25 was obtained for the whole spine, better value than the obtained in previous works[14, 16, 28]. The results reported by Korez et al.[18] and Castro-Mateos et al.[19] were more accurate in the thoracic region but, to evaluate this region, they only included healthy patients. In addition, the development of completely automatic algorithms is still an open problem, being necessary in many cases some degree of user interaction[10–12, 19, 20, 23, 25, 46]. This has been accomplished with the current method, which is fully automatic.

Recently, it has been also conducted a comparative study for vertebra segmentation methods[29]. Five teams entered the study and tested their algorithms on five healthy cases and on five osteoporotic cases with several compression fractures. All methods performed better on the healthy cases. Regarding pathological cases, the performance varied considerably among methods, ranging from 53.8 % to 89.8 % in terms of DSC for the whole spine, lower values than the obtained with the proposed method. The top performers achieved a DSC of 88 % in the upper thoracic region, 89 % in the lower thoracic region and 92 % in the lumbar region; similar performance than the obtained using our method in the thoracic region (88.22 ± 4.41 %) but less accurate in the lumbar region (95.23 ± 1.94%). Also, for most of these methods higher values of MSD were obtained, ranging from 0.64 mm to 5.36 mm.

Regarding atlas-based segmentation methods, the studies related to the construction of spinal atlases are scarcer[46, 47]. The method developed by Hardisty et al.[46] was able to successfully segment tumor-involved vertebrae, but the method required user interaction and they did not consider all thoracic vertebrae. Our yield was similar to the method developed by Forsberg[47]. He achieved a DSC ≥ 95 % for the lumbar and the lower thoracic vertebrae, but he obtained notably worse results in some thoracic vertebrae. They achieved also a higher MSD, with a value of 1.05 ± 0.65 mm. To our knowledge, we have implemented the first probabilistic atlas of the whole spine (last cervical, thoracic and lumbar regions) to refine an initial segmentation with a special focus on ribs suppression. When applying the atlas constructed, it was possible to differentiate between vertebrae and ribs, which in turn allows appropriate removal of these structures while improving the segmentation accuracy on an average of 10 mm in terms of HD. However, when applying the atlas it is necessary to take into account that the initial segmentation is not equally accurate along the spine, so it is necessary to refine more the initial segmentation in some regions than in others. This is the reason why, for the atlas-based segmentation, an adaptive threshold has been used (Fig. 4).

Many anatomical organs and structures have already good segmentation methods based exclusively on the values of the signal provided by the used sensor. The knowledge about anatomical location is mostly provided by neighbourhood relationships between pixels/voxels, which indeed guide the region growing or level-set methods habitually used. Nevertheless, sometimes this knowledge is insufficient because there is no other reason to discard a point than its location with respect to other anatomical structures or the discrepancy with the average or expected resulting shape. These are the cases where using a probabilistic atlas is a sensible choice, and one of them has been shown here. To be useful the atlas must be built to capture the essence of the shape at hand, a goal we have attempted to reach by using the GLM on the values of the distance function. Also, a good registration of the binary shapes used to construct the atlas and a good geometrical adaptation of the atlas to the new case to be segmented is essential. In these cases the anatomical guidance provided by the spinal canal detection has been crucial. The selection of a straight segment of unitary length to perform the registration is a way to avoid the problem of the selection of the reference case, which may influence the results. Besides, it is a way to deal with the problem of having different spinal curvatures and heights.

A drawback of the method is the need to have an enough number of cases manually segmented, a time-consuming and tedious work.

Finally, a marginal consideration must be done about the choice of the metrics for measuring segmentation accuracy; DSC is the most widely accepted but, as this case has shown, it may fail when parts of comparatively small volume are important. Other measures like HD, more related with shape than with volume, are probably more appropriate.

5. CONCLUSIONS

This study presents a new algorithm for the automatic segmentation of the vertebrae from CT images by combining two different segmentation methods. The first uses a level-set method to perform an initial segmentation of the vertebrae, detecting firstly the spinal canal in order to automate the whole process. The second method uses a probabilistic atlas, to both refine the initial segmentation and specifically suppress the ribs or surrounding structures. The algorithm was tested in pathological spines.

In all, the presented method shows accurate and promising results. An accurate spinal segmentation is important due to the high number of pathologies spine-related. Consequently, it can be used to build models for quantification and follow-up of pathologies as well as for surgical planning or treatment planning for radiation therapy, among others.

It remains as an issue for future research how this method can be generalized to other structures for which clear anatomical feature points are of less reliable detection.

Acknowledgements

The authors thank the financial support of the Spanish Ministerio de Economía y Competitividad (MINECO) and FEDER funds under Grants TEC2012-33778 and BFU2015-64380-C2-2-R (D.M.) and DPI2013-4572-R (J.D., E.D.).

Disclosure of Conflicts of Interest

The authors have no relevant conflicts of interest to disclose.

REFERENCES

1. Harris RI, Macnab I. Structural Changes In The Lumbar Intervertebral Discs: Their Relationship to Low Back Pain and Sciatica. *J Bone Joint Surg Br*.1954;36–B(2):304–322.

2. Oliveira MF, Rotta JM, Botelho RV. Survival analysis in patients with metastatic spinal disease: the influence of surgery, histology, clinical and neurologic status. *Arq Neuropsiquiatr*.2015;73(4):330-5.

3. Chou R, Qaseem A, Owens DK, Shekelle P. Diagnostic imaging for low back pain: advice for high-value health care from the American College of Physicians. *Ann Intern Med*.2011;154(3):181-9.

4. Brayda-Bruno M, Tibiletti M, Ito K, et al. Advances in the diagnosis of degenerated lumbar discs and their possible clinical application. *Eur Spine J*.2014;23(3):S315-23.

5. Quattrocchi CC, Santini D, Dell'aia P, et al. A prospective analysis of CT density

measurements of bone metastases after treatment with zoledronic acid. *Skeletal Radiol*.2007;36(12):1121-7.

6. Doi K. Computer-aided diagnosis in medical imaging: historical review, current status and future potential. *Comput Med Imaging Graph*.2007;31(4-5):198-211.

7. Ruiz-España S, Arana E, Moratal D. Semiautomatic computer-aided classification of degenerative lumbar spine disease in magnetic resonance imaging. *Comput Biol Med*.2015;62:196-205.

8. Alomari RS, Ghosh S, Koh J, Chaudhary V. Vertebral Column Localization, Labeling, and Segmentation. *Spinal Imaging and Image Analysis*.2015;18:193-229.

9. Hamarneh G, Li X. Watershed segmentation using prior shape and appearance knowledge. *Image Vis Comput*.2009;27(1-2):59-68.

10. Ghebreab S, Smeulders AW. Combining strings and necklaces for interactive three-dimensional segmentation of spinal images using an integral deformable spine model. *IEEE Trans Biomed Eng*.2004;51(10):1821-9.

11. Mastmeyer A, Engelke K, Fuchs C, Kalender WA. A hierarchical 3D segmentation method and the definition of vertebral body coordinate systems for QCT of the lumbar spine. *Med Image Anal*.2006;10(4):560-77.

12. Rasoulian A, Rohling R, Abolmaesumi P. Lumbar spine segmentation using a statistical multi-vertebrae anatomical shape+pose model. *IEEE Trans Med Imaging*.2013;32(10):1890-1900.

13. Shen H, Litvin A, Alvino C. Localized priors for the precise segmentation of individual vertebras from CT volume data. *Med Image Comput Comput Interv (MICCAI)*.2008;11(1):367-75.

14. Ma J, Lu L. Hierarchical segmentation and identification of thoracic vertebra using

learning-based edge detection and coarse-to-fine deformable model. *Comput Vis Image Underst*.2013;117(9):1072-1083.

15. Kim Y, Kim D. A fully automatic vertebra segmentation method using 3D deformable fences. *Comput Med Imaging Graph*.2009;33(5):343-52.

16. Klinder T, Ostermann J, Ehm M, Franz A, Kneser R, Lorenz C. Automated model-based vertebra detection, identification, and segmentation in CT images. *Med Image Anal*.2009;13(3):471-482.

17. Stern D, Likar B, Pernuš F, Vrtovec T. Parametric modelling and segmentation of vertebral bodies in 3D CT and MR spine images. *Phys Med Biol*.2011;56(23):7505-22.

18. Korez R, Ibragimov B, Likar B, Pernus F, Vrtovec T. A Framework for Automated Spine and Vertebrae Interpolation-Based Detection and Model-Based Segmentation. *IEEE Trans Med Imaging*.2015;34(8):1649-1662.

19. Castro-Mateos I, Pozo JM, Pereañez M, Lekadir K, Lazary A, Frangi AF. Statistical Interspace Models (SIMs): Application to Robust 3D Spine Segmentation. *IEEE Trans Med Imaging*.2015;34(8):1663-1675.

20. Pereañez M, Lekadir K, Castro-Mateos I, Pozo JM, Lazary A, Frangi AF. Accurate Segmentation of Vertebral Bodies and Processes Using Statistical Shape Decomposition and Conditional Models. *IEEE Trans Med Imaging*.2015;34(8):1627-1639.

21. Yao J, O'Connor S, Summers RM. Automated spinal column extraction and partitioning. *IEEE Int Symp Biomed Imaging: from Nano to Macro (ISBI)*.2006;1-3:390-393.

22. Kelm BM, Wels M, Zhou SK, et al. Spine detection in CT and MR using iterated marginal space learning. *Med Image Anal*.2013;17(8):1283-1292.

23. Kang Y, Engelke K, Kalender WA. A new accurate and precise 3-D segmentation

method for skeletal structures in volumetric CT data. *IEEE Trans Med Imaging*.2003;22:586-598.

24. Huang J, Jian F, Wu H, et al. An improved level set method for vertebra CT image segmentation. *Biomed Eng Online*.2013;12(1):48.

25. Lim PH, Bagci U, Bai L. Introducing Willmore flow into level set segmentation of spinal vertebrae. *IEEE Trans Biomed Eng*.2013;60(1):115-22.

26. Tan S, Yao J, Ward M, Summers RM. 3D Multi-scale level set segmentation of vertebrae. *IEEE Int Symp Biomed Imaging: from Nano to Macro (ISBI)*.2007;896–899.

27. Ruiz-España S, Díaz-Parra A, Arana E, Moratal D. A Fully Automated level-set based segmentation method of thoracic and lumbar vertebral bodies in Computed Tomography images. *Conf Proc IEEE Eng Med Biol Soc (EMBC)*.2015;2015:3049-3052.

28. Forsberg D, Lundström C, Andersson M, Knutsson H. Model-based registration for assessment of spinal deformities in idiopathic scoliosis. *Phys Med Biol*.2014;59(2):311-26.

29. Yao J, Burns J, Forsberg D, et al. A Multi-center Milestone Study of Clinical Vertebral CT Segmentation. *Comput Med Imaging Graph*.2016;49:16-28.

30. Steger S, Kirschner M, Wesarg S. Articulated atlas for segmentation of the skeleton from head & neck CT datasets. *IEEE Int Symp Biomed Imaging: from Nano to Macro (ISBI)*.2012;1256-1259.

31. Shi C, Wang J, Cheng Y. Sparse Representation-Based Deformation Model for Atlas-Based Segmentation of Liver CT Images. *Image Graph*.2015;9219:410-419.

32. Domingo J, Dura E, Ayala G, Ruiz-España S. Means of 2D and 3D Shapes and Their Application in Anatomical Atlas Building. *Comput Anal Images Patterns*.2015;9256:522-533.

33. Ruiz-España S, Domingo J, Díaz-Parra A, et al. Automatic Segmentation of the Spine

by Means of a probabilistic Atlas With a Special Focus on Ribs Supression. Preliminary Results. *Conf Proc IEEE Eng Med Biol Soc (EMBC)*.2015;2015:2014-2017.

34. Park H, Bland PH, Meyer CR. Construction of an abdominal probabilistic atlas and its application in segmentation. *IEEE Trans Med Imaging*.2003;22(4):483-92.

35. Cabezas M, Oliver A, Lladó X, Freixenet J, Cuadra MB. A review of atlas-based segmentation for magnetic resonance brain images. *Comput Methods Programs Biomed*.2011;104(3):158-177.

36. Fortunati V, Verhaart RF, van der Lijn F, et al. Tissue segmentation of head and neck CT images for treatment planning: a multiatlas approach combined with intensity modeling. *Med Phys*.2013;40(7):71905.

37. Zhuang X, Bai W, Song J, et al. Multiatlas whole heart segmentation of CT data using conditional entropy for atlas ranking and selectio. *Med Phys*.2015;42(7):3822-3833.

38. Dura E, Domingo J, Rojas-Arboleda AF, Martí-Bonmatí L. Mean sets for building 3D probabilistic liver atlas from perfusion MR images. *Int Conf on Image Processing Theory, Tools and Applications (IPTA)*.2012:186-191.

39. Zhou J, Yan Z, Lasio G, et al. Automated compromised right lung segmentation method using a robust atlas-based active volume model with sparse shape composition prior in CT. *Comput Med Imaging Graph*.2015;46(1):47-55.

40. Chu C, Oda M, Kitasaka T, et al. Multi-organ segmentation based on spatially-divided probabilistic atlas from 3D abdominal CT images. *Med Image Comput Comput Interv (MICCAI)*.2013;8150:165-72.

41. Linguraru MG, Sandberg JK, Li Z, Shah F, Summers RM. Automated segmentation and quantification of liver and spleen from CT images using normalized probabilistic atlases and enhancement estimation. *Med Phys*.2010:37(2):771-783.

42. Xu Y, Xu C, Kuang X, et al. 3D-SIFT-Flow for atlas-based CT liver image segmentation. *Med Phys*.2016;43(5):2229-2241.

43. Michopoulou SK, Costaridou L, Panagiotopoulos E, Speller R, Panayiotakis G, Todd-Pokropek A. Atlas-based segmentation of degenerated lumbar intervertebral discs from MR images of the spine. *IEEE Trans Biomed Eng*.2009;56(9):2225-2231.

44. Taso M, Le Troter A, Sdika M, et al. Construction of an in vivo human spinal cord atlas based on high-resolution MR images at cervical and thoracic levels: preliminary results. *Magn Reson Mater Phy*.2014;27(3):257-67.

45. Lévy S, Benhamou M, Naaman C, Rainville P, Callot V, Cohen-Adad J. White matter atlas of the human spinal cord with estimation of partial volume effect. *Neuroimage*.2015;119:262-271.

46. Hardisty M, Gordon L, Agarwal P, Skrinskas T, Whyne C. Quantitative characterization of metastatic disease in the spine. Part I. Semiautomated segmentation using atlas-based deformable registration and the level set method. *Med Phys*.2007;34(8):3127.

47. Forsberg D. Atlas-based registration for accurate segmentation of thoracic and lumbar vertebrae in CT data. *Recent Adv Comput Methods Clin Appl Spine Imaging*.2015;20:49-59.

48. Ibañez MV, Schroeder W, Cates L. Insight software Consortium. The ITK Software Guide. http://www.itk.org/ItkSoftwareGuide.pdf. Accessed June 15, 2016.

49. Loader C. R package: Local regression, likelihood and density estimation. CRAN repository 2013. http://cran.r-project.org/web/packages/locfit. Accessed June 15, 2016.

50. Park H, Hero A, Bland P, Kessler M, Seo J, Meyer C. Construction of abdominal probabilistic atlases and their value in segmentation of normal organs in abdominal CT

scans. *IEICE Trans Info and Syst*.2010;E93-D(8):2291-2301.

51. Pohl KM, Fisher J, Bouix S, et al. Using the logarithm of odds to define a vector space on probabilistic atlases. *Med Image Anal*.2007;11(5):465-77.

52. Stoyan D, Stoyan H. *Fractals, Random Shapes and Point Fields : Methods of Geometrical Statistics*. Wiley;1994.

53. Baddeley A, Molchanov I. Averaging of Random Sets Based on Their Distance Functions. *J Math Imaging Vis*.1998;8(1):79-92.

54. Díaz-Parra A, Arana E, Moratal D. A fully automated method for spinal canal detection in computed tomography images. *Conf Proc IEEE Eng Med Biol Soc (EMBC)*.2014;2014:5514-7.

55. De Bruijne M, van Ginneken B, Viergever MA, Niessen WJ. Adapting Active Shape Models for 3D Segmentation of Tubular Structures in Medical Images. *Inf Process Med Imaging*.2003;18:136–147.

56. Zhang K, Zhang L, Song H, Zhou W. Active contours with selective local or global segmentation: A new formulation and level set method. *Image Vis Comput*.2010;28(4):668-676.

57. Kalpathy-Cramer J, Awan M, Bedrick S, Rasch CRN, Rosenthal DI, Fuller CD. Development of a software for quantitative evaluation radiotherapy target and organ-at-risk segmentation comparison. *J Digit Imaging*.2014;27(1):108-19.

58. Huttenlocher DP, Klanderman GA, Rucklidge WJ. Comparing images using the Hausdorff distance. *IEEE Trans Pattern Anal Mach Intell*.1993;15(9):850-863.

59. Aspert N, Santa-Cruz D, Ebrahimi T. Mesh : Measuring errors between surfaces using the Husdorff distance. *Proc IEEE Int Conf Multimed Expo (ICME).2002*;1:705-708.